Physica Scripta. Vol. T109, 54–60, 2004

Applications of Time-Dependent Density Functional Theory

Silvana Botti*

Laboratiore des Solides Irradiés, CNRS-CEA-École Polytechnique, F-91128 Palaiseau, France

Received May 6, 2003; accepted July 15, 2003

PACS ref: 71.10.–w, 71.15.Qe, 71.35.Cc, 78.20.Bh

Abstract

The progress of experimental techniques makes more and more precise measurements available. Their interpretation requires improved theoretical tools. The time-dependent density functional theory (TDDFT) allows to study electronic excitations involved in spectroscopic experiments, possibly conserving a computational effort comparable to that of ground-state density functional theory. I will present some applications of TDDFT to the calculation of absorption and electron energy loss spectra in extended and finite systems, discussing the advantages and the limits of different approximation schemes.

1. Introduction

Density functional theory (DFT) [1,2] is nowadays a standard many-body approach for first principle calculations. Thanks to its generality, it is applied in atomic, molecular, solid state, nuclear physics and quantum chemistry, providing an efficient and accurate description of *ground state properties*—such as total energies, atomic structures, elastic constants, phonon spectra—in a large class of systems. It is well known that, in its static formulation, DFT is not designed to access *excited states*. Nevertheless, there is a strong interest in the theoretical study of excitations, as they are, e.g., at the basis of many electronic and opto-electronic technological developments and they are involved in spectroscopic experiments investigating the physical properties of materials. In the recent years, the continuous improvements of experimental techniques have made new measurements available, whose resolution has drastically increased. Meanwhile, the naive theoretical tools (i.e., the simple one-particle transition picture) have definitely shown to give too poor reference spectra, inadequate to interpret and predict, sometimes even qualitatively, processes occurring in experiments. Instead, precise calculations can provide an essential contribution to extract the information hidden in measured spectra, e.g., explaining the origin of observed peaks. To illustrate this concept, we can consider the characterization of a surface: the comparison between optical measurements and realistic spectra, computed for different reconstruction schemes, has become a non-destructive tool to identify the atomic positions on the surface [3]. Moreover, it is clear that only reliable calculations acquire a predictive power, to be used in the design of new materials of technological interest.

One possibility to overcome the intrinsic limits of static DFT is offered by its natural extension to the case of time-dependent electronic densities, the time-dependent DFT (TDDFT) [4–7]. By analogy with classical mechanics, as the static DFT ground state is determined by the total energy minimum, the evolution of the system in response to an external time-dependent perturbation is obtained by looking for the extrema of the quantum-mechanical action functional, yielding a time-dependent version of the Kohn–Sham (KS) equations. Other approaches commonly used in chemistry and solid state physics, the configuration interaction method [8] and methods based on solving the Bethe–Salpeter equation (BSE) within the GW approximation [9–13], suffer from a high numerical cost, which at present prevents applications to very complex systems. Unlike these demanding techniques, in some of the approximations used (e.g., the adiabatic local density approximation TDLDA), the TDDFT has the advantage to require a computational effort comparable to that of static DFT. In principle, it is a correct and general theory for neutral excitations (i.e., which do not change the number of electrons), but in practice, its use is still restricted to some classes of systems, due to the difficulty to find general approximations for the *unknown* exchange-correlation (xc) contributions: the xc-potential V_{xc} and its variation with respect to density, the xc-kernel f_{xc}. Recently, there have been several attempts to overcome these limitations and extensive discussions can be found in Ref. [14].

In this lecture I want to discuss some applications of TDDFT to the calculation of the optical properties of a variety of systems: from clusters and nanostructured materials, to bulk semiconductors and transition-metal oxides. We will see that satisfactory calculations, in agreement with experiments, require not only a proper description of the electronic states, but also the account of the microscopic inhomogeneity of the system and the inclusion of effective many-body interactions. After a brief introduction to the formalism, a selection of calculated spectra will be presented, in an order given by the increasing level of the underlying approximations. Results in good agreement with experiments do not necessarily come from a single approximation scheme. To clarify this point, I will focus on why and to which extent each term in the TDDFT equations is associated to specific physical effects, in view of the characteristics of the studied system, in order to conclude in which case that term gives a relevant contribution or can be neglected.

2. Spectroscopic experiments and calculation of dielectric functions

In the following presentation, only two types of experiments involving neutral excitations will be considered:

* e-mail: silvana.botti@polytechnique.fr

With contributions from Apostolos Marinopoulos, Valerio Olevano, Lucia Reining, Francesco Sottile and Nathalie Vast.

optical absorption and electron energy loss spectroscopy (EELS). The *absorption* spectrum is described by the imaginary part of the macroscopic dielectric function $\varepsilon_M(\omega)$. Calculations based on an Hamiltonian description of the electronic systems, give directly access to their microscopic dielectric response $\varepsilon(\boldsymbol{r}, \boldsymbol{r}'; \omega)$, which needs to be properly related to the measured macroscopic response. In the case of periodic systems, it can be convenient to move to the reciprocal space, where the Fourier transform of the microscopic dielectric function is a $\boldsymbol{G}, \boldsymbol{G}'$-matrix (where $\boldsymbol{G}$-vectors are reciprocal lattice vectors), depending on a wavevector $\boldsymbol{q}$ belonging to the first Brillouin zone: $\varepsilon_{\boldsymbol{G},\boldsymbol{G}'}(\boldsymbol{q}, \omega)$. Neglecting the off-diagonal elements of $\varepsilon_{\boldsymbol{G},\boldsymbol{G}'}$ is equivalent, in the direct space, to state that the microscopic dielectric function $\varepsilon(\boldsymbol{r}, \boldsymbol{r}', \omega)$ does not depend explicitly on the positions $\boldsymbol{r}$ and $\boldsymbol{r}'$, but simply on the distance $\boldsymbol{r} - \boldsymbol{r}'$, as if the system were homogeneous. This assumption leads to a macroscopic dielectric function in the form of the spatial average of the microscopic dielectric function:

$$\varepsilon_M^{NLF}(\omega) = \lim_{q \to 0} \varepsilon_{0,0}(\boldsymbol{q}, \omega). \tag{1}$$

In fact, the off-diagonal terms in the dielectric matrix reflect the non-homogeneity of the space, as they account for the fact that a perturbing field of wave vector $\boldsymbol{q}$ and frequency ω induces microscopic fields with $(\boldsymbol{q} + \boldsymbol{G}, \omega)$ components. The frequency ω is not affected because of the homogeneity of the time. When all matrix elements are properly considered, the macroscopic dielectric function ε_M can be deduced by the formula due to Adler and Wiser [15–17]:

$$\varepsilon_M(\omega) = \lim_{q \to 0} \frac{1}{\varepsilon^{-1}_{\boldsymbol{G}=\boldsymbol{G}'=0}(\boldsymbol{q}, \omega)}. \tag{2}$$

The difference between Eq. (2) and its counterpart for an homogeneous system Eq. (1) constitutes the so-called *crystal local field effect* (LFE) corrections [18]. In general, for anisotropic systems, Eqs. (2) and (1) depend on the direction of the vector $\boldsymbol{q}$ (i.e., on the polarization of the incoming radiation), thus both microscopic and macroscopic responses are described by a dielectric tensor, instead of simple scalar functions. We should keep in mind that, for the case of non-isotropic media, also LFE may depend on light-polarization.

An *electron energy loss* experiment consists in the excitation of electron–hole pairs, plasmons and other high-order multipair excitations by means of the energy lost by an electron impinging on the sample. The electron energy loss function for a transferred momentum $\boldsymbol{q} + \boldsymbol{G}$ is given by [19]:

$$L_{\boldsymbol{q}+\boldsymbol{G}}(\omega) = -\mathrm{Im}\left[\varepsilon^{-1}_{\boldsymbol{G},\boldsymbol{G}}(\boldsymbol{q}, \omega)\right]. \tag{3}$$

Neglecting LFE, we obtain the simplified form:

$$L^{NLF}_{\boldsymbol{q}+\boldsymbol{G}}(\omega) = -\mathrm{Im}\left[\frac{1}{\varepsilon_{\boldsymbol{G},\boldsymbol{G}}(\boldsymbol{q}, \omega)}\right]. \tag{4}$$

Hence, we conclude that in both kind of spectroscopies, all the information we need to reproduce measured spectra can be extracted from the microscopic dielectric function (or tensor) $\varepsilon_{\boldsymbol{G},\boldsymbol{G}'}(\boldsymbol{q}, \omega)$, more precisely from its inverse matrix $\varepsilon^{-1}_{\boldsymbol{G},\boldsymbol{G}'}(\boldsymbol{q}, \omega)$.

Let us move some further steps in the development of calculations within TDDFT. The inverse of the dielectric function ε^{-1} can be expressed in terms of another important quantity, the irreducible polarizability χ

$$\varepsilon^{-1}(\boldsymbol{r}, \boldsymbol{r}', \omega) = \delta(\boldsymbol{r} - \boldsymbol{r}') + \int \mathrm{d}\boldsymbol{r}'' v(\boldsymbol{r} - \boldsymbol{r}'') \chi(\boldsymbol{r}'', \boldsymbol{r}', \omega), \tag{5}$$

where v is the bare coulomb interaction. The polarizability χ describes the linear response of the charge density to an external time-dependent perturbation $V_{ext}(\boldsymbol{r}', t')$:

$$\chi(\boldsymbol{r}, t, \boldsymbol{r}', t') = \left.\frac{\delta\rho(\boldsymbol{r}, t)}{\delta V_{ext}(\boldsymbol{r}', t')}\right|_{V_{ext}=0}. \tag{6}$$

In the Kohn–Sham (KS) scheme, the independent-particle polarizability χ_0 of a fictitious non-interacting system relates, in a fully equivalent way, the electron density $\rho(\boldsymbol{r}, t)$ to the one-particle effective potential $V_{eff}(\boldsymbol{r}, t)$:

$$\chi_0(\boldsymbol{r}, t, \boldsymbol{r}', t') = \left.\frac{\delta\rho(\boldsymbol{r}, t)}{\delta V_{eff}(\boldsymbol{r}', t')}\right|_{V_{eff}=0}. \tag{7}$$

Remembering the definition of the effective potential $V_{eff}(\boldsymbol{r}, t) = V_{ext}(\boldsymbol{r}, t) + V_H(\boldsymbol{r}, t) + V_{xc}(\boldsymbol{r}, t)$, where V_H and V_{xc} denote the Hartree and the exchange-correlation time-dependent potentials, it is easy to obtain

$$\frac{\delta V_{eff}(\boldsymbol{r}, t)}{\delta V_{ext}(\boldsymbol{r}', t')} = \delta(\boldsymbol{r} - \boldsymbol{r}')\delta(t - t') + \iint \left[\frac{\delta(t - t'')}{|\boldsymbol{r} - \boldsymbol{r}''|} + f_{xc}(\boldsymbol{r}, t, \boldsymbol{r}'', t'')\right] \chi(\boldsymbol{r}'', t'', \boldsymbol{r}', t')\, \mathrm{d}\boldsymbol{r}''\, \mathrm{d}t'', \tag{8}$$

where

$$f_{xc}(\boldsymbol{r}, t, \boldsymbol{r}', t') = \left.\frac{\delta V_{xc}[\rho(\boldsymbol{r}, t)]}{\delta\rho(\boldsymbol{r}', t')}\right|_{V_{ext}=0} \tag{9}$$

is the time-dependent *xc-kernel* and

$$\frac{\delta V_H[\rho(\boldsymbol{r}, t)]}{\delta\rho(\boldsymbol{r}', t')} = \frac{\delta(t - t')}{|\boldsymbol{r} - \boldsymbol{r}'|} \tag{10}$$

accounts for the variation of the Hartree potential, which contains what we have already called *crystal local field* effects. A Dyson-like screening equation [20] connecting the two polarizabilities χ and χ_0, follows in a straightforward way from Eqs. (6), (7) and (9):

$$\chi(\boldsymbol{r}, \boldsymbol{r}', \omega) = \chi_0(\boldsymbol{r}, \boldsymbol{r}', \omega) + \int \mathrm{d}\boldsymbol{r}_1\, \mathrm{d}\boldsymbol{r}_2 \chi_0(\boldsymbol{r}, \boldsymbol{r}_1, \omega) \left[\frac{1}{|\boldsymbol{r}_1 - \boldsymbol{r}_2|} + f_{xc}(\boldsymbol{r}_1, \boldsymbol{r}_2, \omega)\right] \chi(\boldsymbol{r}_2, \boldsymbol{r}', \omega). \tag{11}$$

Provided one can find a satisfactory approximation for the xc-kernel, it is possible to calculate χ (and hence ε^{-1}) from Eq. (11). In fact, χ_0 has the well known independent-particle form obtained by Adler [15] and Wiser [16]

$$\chi_0(\boldsymbol{r}, \boldsymbol{r}', \omega) = \sum_{ij} 2(f_i - f_j) \frac{\psi_i(\boldsymbol{r})\psi_j^*(\boldsymbol{r})\psi_j(\boldsymbol{r}')\psi_i^*(\boldsymbol{r}')}{\omega - \omega_{ij} + \mathrm{i}\eta}. \tag{12}$$

with $\omega_{ij} = (\varepsilon_j - \varepsilon_i)$. In Eq. (12) (i, j) label the electronic states ψ_i, ψ_j of energy $\varepsilon_i, \varepsilon_j$, coming from the solution of the static Kohn–Sham equations, and f_i, f_j are Fermi occupation numbers. The small imaginary constant η added in the denominator accounts for causality and can describe lifetime effects; the factor 2 stems from spin degeneracy. At this stage, a first approximation has already been employed in the KS equations to express the static V_{xc} potential. We point out that if the exact $V_{xc}(\omega)$ were known, the xc-kernel f_{xc} would naturally follow from its functional derivative. However, we adopt an approximate expression for V_{xc}, and the form of f_{xc} is not restrained to satisfy the functional derivative relation. Concerning V_{xc}, in the following we will always deal with the Local Density Approximation (LDA) [2].

Equation (11) relates the linear response of an interacting system in terms of the response of a non-interacting KS system with external potential $V_{eff}(\boldsymbol{r}, t)$. While the Hartree kernel (10) in Eq. (11), is simply the variation of the Hartree potential with respect to the electron density and can be calculated formally *exactly*, the analytic expression for the xc-kernel is unknown, and the application of the theory has to rely on some approximations. The lowest level of approximation, widely employed in actual calculations, which corresponds to the Random Phase Approximation (RPA) [15,16] of the Lindhard theory of screening, consists in neglecting the xc-kernel:

$$f_{xc}^{RPA} = 0. \tag{13}$$

If also LFE are neglected within RPA, the calculation of absorption reduces to the naive independent-particle transition picture of the Fermi's golden rule. This can be easily seen by exploiting a different form of Eq. (2), namely [21]:

$$\varepsilon_M(\omega) = \lim_{q\to 0} (1 - v_0(\boldsymbol{q})\bar{\chi}(\boldsymbol{q}, \boldsymbol{G} = 0, \boldsymbol{G}' = 0, \omega)), \tag{14}$$

with $\bar{\chi} = \chi_0 + \chi_0(\bar{v} + f_{xc})\bar{\chi}$. Here, $\bar{\chi}$ is a modified response function and $\bar{v}$ a modified Coulomb interaction, defined by $\bar{v}_{\boldsymbol{G}}(\boldsymbol{q})$ which equals $v_{\boldsymbol{G}}(\boldsymbol{q})$ for all $\boldsymbol{G}$, except for the long-range term $\bar{v}_{\boldsymbol{G}=0}(\boldsymbol{q})$ which is zero. If we include neither xc-contributions ($f_{xc} = 0$) nor LFE ($\bar{v} = 0$), we obtain immediately

$$\varepsilon_M(\omega) = \lim_{\boldsymbol{q}\to 0} (1 - v_0(\boldsymbol{q})\chi_0(\boldsymbol{q}, \boldsymbol{G} = 0, \boldsymbol{G}' = 0, \omega)),$$

which equals Eq. (1). Referring to this approximation, we will use the definition independent-particle RPA (IP-RPA), otherwise we will take for granted the inclusion of LFE in RPA.

Another simple form for the xc-kernel is the adiabatic local density approximation (TDLDA) [5,6,22], where a static local kernel is derived from the LDA exchange-correlation potential used in ground state calculations:

$$f_{xc}^{TDLDA}(\boldsymbol{r}, \boldsymbol{r}') = \delta(\boldsymbol{r}, \boldsymbol{r}') \frac{\mathrm{d}V_{xc}^{LDA}(\boldsymbol{r})}{\mathrm{d}\rho(\boldsymbol{r})}. \tag{15}$$

As we will see in the next section, TDLDA has turned out to yield only slight modifications to RPA results in many applications, in particular in solids, being thus inadequate to correct RPA results in case they are completely unsatisfactory.

More in general, in order to go beyond the RPA, further terms have to be included in f_{xc}. These terms can be discussed in a quasi-particle picture as stemming from electron–electron and electron–hole interactions. The electron-electron interaction intervenes in the definition of *quasi-particle* states. The KS eigenvalues are never meant to describe electron addition and removal energies for the interacting system: it is well known that the KS theory systematically underestimates photoemission gaps. They can be corrected by replacing the KS equation by a corresponding equation within the Green's function many-body formalism. The optical gaps need a further correction: in a neutral excitation, as the excited electron does not leave the system, it continues interacting with the hole left behind in the valence state, creating an electron–hole pair (*exciton*). Depending on the intensity of the electron–hole interaction, excitons can lead to bound states within the gap and/or to strong deformations above the continuum absorption edge. The importance of these effects depends on the size of the screening of the electron–hole interaction and on the details of the band structure. Alternatively in TDDFT, the optical gap is determined by the KS potential, yielding KS eigenvalues, plus the sum of quasi-particle and excitonic contributions due to the variations of the KS potential, taken into account through the xc-kernel. Of course, partial cancellations occur in this sum, so that neither of the two contributions has to be described completely in TDDFT.

At present in the field of TDDFT a fervent discussion is directed to find more satisfying approximations for the xc-kernel f_{xc}, aiming in particular at improving absorption spectra in solids, which are often poorly described both within RPA and TDLDA. Progresses in the description of xc-contributions are expected to come from a better understanding of the differences between the spectroscopic properties of finite and infinite systems, as well as the differences between calculated absorption and EELS in the same system.

3. Some applications

In this Section I will illustrate some examples of TDDFT calculations. All presented applications start with a DFT ground state calculation within the Local Density Approximation (LDA), using norm-conserving pseudopotentials and a basis of plane waves (except for the case of small clusters, where an implementation in real space was employed). First, I want to discuss the role of LFE, by focusing on comparisons between experimental data and some calculations obtained both at the level of approximation of the Fermi's golden rule for independent particle transitions (IP-RPA, thus without LFE), and in standard RPA (including LFE). We have already explained that LFE show up when the material is non-homogeneous, now we want to investigate how their intensity measures the degree of inhomogeneity of the system.

To this end, we display in Fig. 1 the loss function of graphite calculated by Marinopoulos *et al*. [23]. Graphite is an hexagonal quasi-two-dimensional system, characterized by a layered structure with a weak interplane interaction

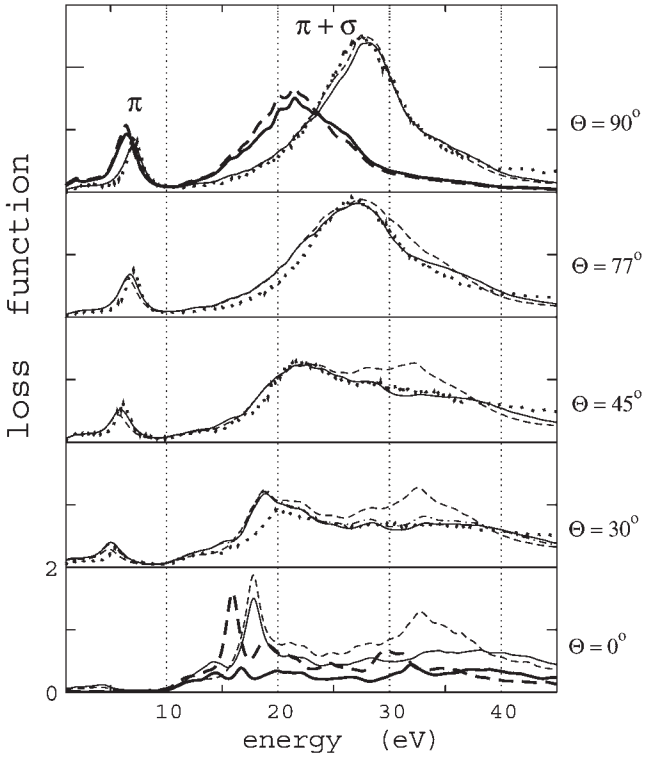

Fig. 1. Electron energy loss functions of graphite for different orientation angles between the momentum-transfer $\boldsymbol{q}$ (for $q = 0.25\,\text{Å}^{-1}$) and the graphite c-axis, from Ref. [23]. Dashed lines are obtained without, solid lines including LFE within the RPA. Experimental results are indicated by the dotted lines. In the $\Theta = 30^\circ$ spectrum the dot-dashed curve is the TDLDA result. The thick lines denote the results with a double spacing between graphene layers.

and a very strong in-plane bonding. As a consequence, its dielectric response is anisotropic: $\varepsilon(\boldsymbol{q}, \omega)$ depends on the orientation Θ of the momentum transfer $\boldsymbol{q}$ with respect to the crystallographic c-axis, perpendicular to the layers. The loss function was determined in RPA with LFE (solid lines) and without LFT (dashed lines) for a wide range of momentum-transfer $\boldsymbol{q}$ orientations. For $\Theta = 90^\circ$, when the $\boldsymbol{q}$ vector lies in the plane of the layers, LFE are found to be extremely small. With or without their inclusion, the plasmon positions and the line shapes are in excellent agreement with experiment. While the orientation of $\boldsymbol{q}$ gets closer to the c-axis, not only the EELS spectra change significantly, due to the relevant anisotropy of the dielectric response, but also the importance of LFE increases continuously. Finally, for $\Theta \leq 45^\circ$ only the RPA result remains close to the experimental curves. We can explain this outcome by observing that the electron density is delocalized on each graphene plane, and thus the density experienced by the in-plane $\boldsymbol{q}$ vector is relatively homogeneous; instead the electron density is clearly inhomogeneous in the direction parallel to the c-axis, due to the stacking of graphene layers, which prevents from neglecting LFE.

Another example of multilayered system is offered by semiconductor superlattices (SLs). These heterostructures are constructed by alternating layers of two different constituents by epitaxial growth techniques. Botti *et al.* [24] studied the zero-frequency dielectric tensor of $(GaAs)_p/(AlAs)_p$ superlattices, grown in the [001] direction. GaAs and AlAs have zincblende structures with almost the same lattice parameter a. In the superlattice, the reduction of the originally cubic symmetry gives rise to a dielectric anisotropy, which depends in a non-trivial way on the layer width pa, where p is the number of planes constituting each layer. The possibility to control the anisotropy of the optical response through the manufacturing of these artificial materials have been exploited to generate optical frequency conversion [25]. Figure 2 shows the two components of the static dielectric tensor, for light polarized in the growth direction $\varepsilon_\parallel$ and in the plane perpendicular to the growth direction $\varepsilon_\perp$, as a function of the SL period p. The curves in the upper panel of Fig. 2 refer to IP-RPA calculations, which neglect LFE. For small SL periods, the differences between the two components are related to quantum-confinement effects. For large SL periods, ε tends to the average of the bulk dielectric constants of GaAs and AlAs calculated without LFE (arrow on the upper panel of Fig. 2). This occurs for both polarizations, so that the birefringence $\Delta n = \sqrt{\varepsilon_\perp} - \sqrt{\varepsilon_\parallel}$, which measures the anisotropy of the dielectric response, tends to zero. This theoretical prediction is completely misleading, as a vanishing birefringence is not only in disagreement with experimental data, but also with the classical limit given by the effective medium theory. In fact, for large layer widths, quantum-confinement effects vanish and the birefringence can be determined by the classic Maxwell's equations. The lower panel of Fig. 2 shows the same quantities calculated including LFE. As it usually happens also in bulk systems, LFE decrease the absolute value of the dielectric tensor components. The LFE are shown in the inset of Fig. 2: for an in-plane light polarization, they are found to be almost constant with the period, in particular they are equal to the average of LFE corrections to the dielectric constants of bulk GaAs and AlAs. This is consistent with

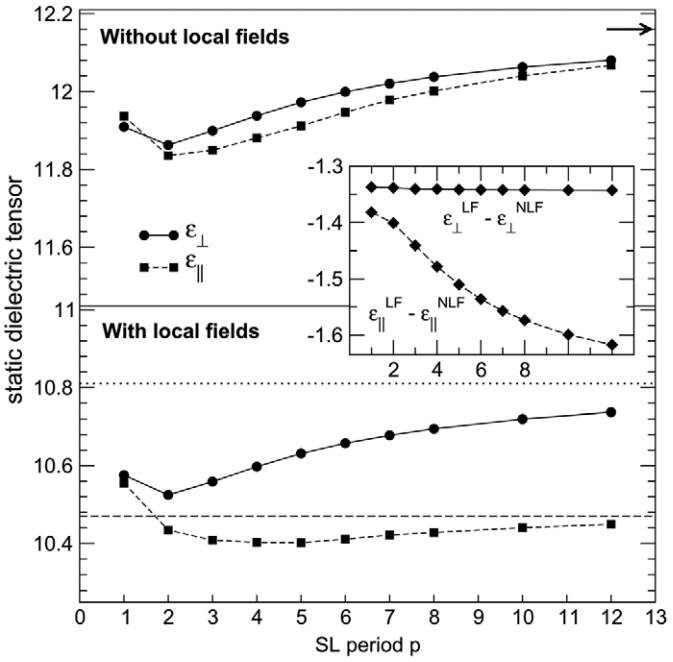

Fig. 2. RPA static dielectric tensors of $(GaAs)_p/(AlAs)_p$ SLs calculated without (ε^{NLF}, upper panel) and with (ε^{LF}, lower panel) LFE and their difference (inset), as a function of the SL period p from Ref. [24]. Arrow: average of bulk GaAs and AlAs dielectric constants, calculated without LFE. Dotted (dashed) line: classical effective medium value of $\varepsilon_\perp(\varepsilon_\parallel)$.

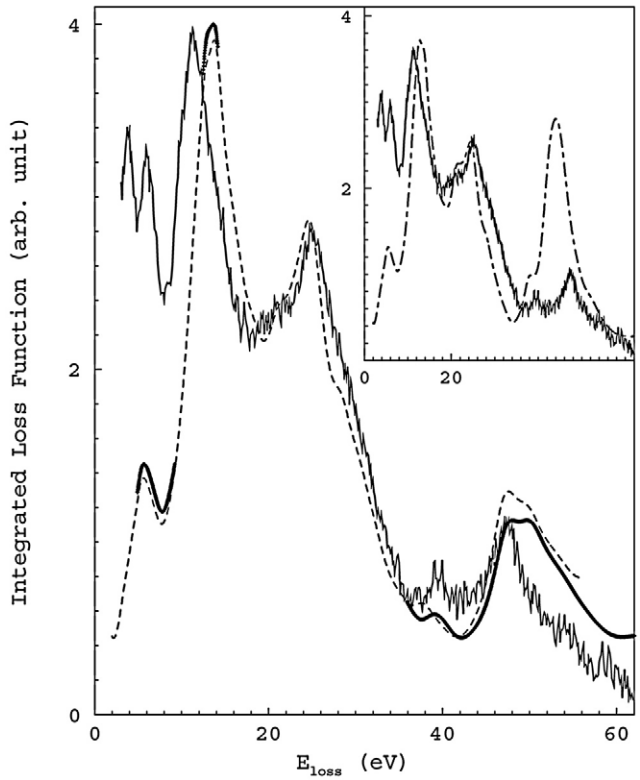

Fig. 3. Integrated loss function of TiO_2 at $\mathbf{q} \approx 0.4\,\text{Å}^{-1}$ from Ref. [26]. Solid line: Experiment. Dashed line: RPA results. Thick solid line: TDLDA calculations. In the inset the dot-dashed line indicates the theoretical results without LFE.

the fact that the multilayer structure is not "seen" in plane. On the other hand, for increasing p, LFE give increasingly negative contributions in the direction which crosses the interfaces, where the inhomogeneity of the medium is brought into play. Thanks to the anisotropy of LFE, the birefringence undergoes a steep rise in the small-medium period region, reaching a finite plateau value for large SL periods, in agreement both with the experimental data and the classical effective medium theory.

In the previous examples, the effects of inhomogeneity were related to the geometric structure of the system. However, the inhomogeneity can also come from the localization of the electronic levels involved in excitations. Vast *et al.* [26] studied the role of LFE in the description of EELS spectra of rutile TiO_2, a transition-metal oxide. In Fig. 3 we show the integrated loss function for $\boldsymbol{q}$ oriented in the [110] direction ($q \approx 0.4\,\text{Å}^{-1}$), in an energy range up to 60 eV, which concerns electron transitions from valence and semi-core Ti (3p) states. In fact, as it happens in various compounds of 3d transition metals, although the 3p states are almost atomic-like, still they can slightly hybridize due to the interaction with neighboring atoms. The RPA spectrum without LFE yields results which are very similar to those obtained including LFE up to 25 eV. At higher energies, the theoretical peak calculated using Eq. (4) can not describe correctly the main structure at $\simeq 47$ eV, which is originated by transitions from the semi-core states: LFE reduce the intensity and blue-shift by more than 6 eV the semi-core peak, allowing the final excellent agreement with experimental data. Once again LFE turn out to be crucial: when semi-core excitations are concerned, they allow to account for the strong inhomogeneity due to the presence of almost atomic-like localized states.

The applications discussed up to now could lead to the erroneous believing that the independent-particle transitions described by χ_0, together with the transition mixing induced by the bare Coulomb interaction are always sufficient to reproduce all spectroscopic measurements. This would imply that quasi-particle corrections and excitonic effects must cancel each other almost exactly, therefore it would be useless to include further many-body corrections through the xc-kernel f_{xc}. This is in general not true. To supply an evidence, we will consider the apparently simple calculation of the absorption spectrum of bulk silicon. In Fig. 4 we display the imaginary part of the macroscopic dielectric function $\varepsilon_M(\omega)$ of silicon [27,28]. Concerning the peak positions and their relative intensities, IP-RPA calculations (dashed line), do not differ significantly from RPA calculations (dotted line), in which LFE have been switched on. This occurrence is not surprising, if we look back at the considerations about the relation between LFE and the inhomogeneity of the medium: as silicon charge density does not exhibit a particularly strong inhomogeneity, it is reasonable to expect not too drastic local field corrections. The discrepancies with respect to the experiment of both IP-RPA and RPA curves are well-known [12,29]: theoretical peak positions are red-shifted and the intensity of the first peak (E_1) is strongly underestimated. The case of silicon is not an exception: a mediocre quality is revealed by a variety of absorption spectra in extended systems.

These considerations lead us to consider how the existing approximation schemes include xc-contributions in the dielectric response of electronic systems. The TDLDA xc-kernel (15) has been successfully applied to atoms, small

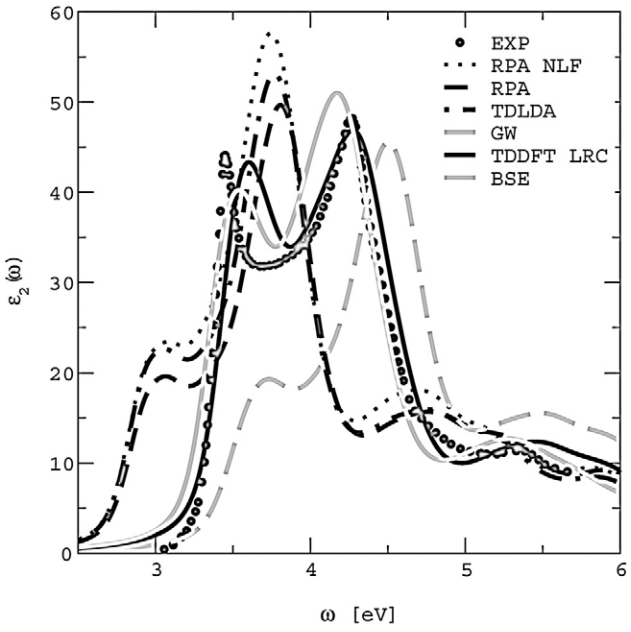

Fig. 4. Imaginary part of the macroscopic dielectric function of Silicon from Refs. [27,28]. Dots: experiment; dotted line: RPA calculations without LFE (Fermi's golden rule); dashed line: RPA calculations including LFE, dot-dashed line: TDLDA calculations; long-dashed grey line: GW-RPA calculations; solid grey line: BSE calculations; solid line: LRC calculations, where a good fit to experiment is obtained using $\alpha = 0.2$.

molecules, metallic and semiconductor clusters, fullerenes [30]: despite some problematic cases (e.g., the calculation of Rydberg series), the calculated excitation energies and absorption spectra have turned out to be in good agreement with the available experimental data. As an example, the absorption spectra of some Na_n clusters obtained by Vasiliev *et al.* [31,32] are illustrated in Fig. 5, where IP-PRA calculations (dotted lines) are compared to TDLDA results (solid lines). Experimental spectra are also plotted (dashed lines). As a general feature, which can be remarked in all metallic and semiconductor cluster, the TDLDA peaks are blue-shifted with respect to the IP-RPA peaks: as a result, the photoabsorption thresholds are displaced to higher energies, in agreement with experiments, and transition energies are accurately reproduced.

In view of these promising results for clusters, a first attempt to explore xc-contributions in solids is the inclusion of the TDLDA xc-kernel. We can see in Fig. 4 that TDLDA (dash-dotted line) induces some minor modifications to the RPA curve, so that no real improvement can be detected. On the other hand, Olevano and Reining [14,33] have proved for the EELS spectrum of silicon that the TDLDA approximation gives an excellent agreement with experiment, even if the curve is only slightly modified in comparison to the RPA curve. It is interesting to remark that the similarity between RPA and TDLDA results holds also for the loss function of graphite, as shown in the panel for $\Theta = 30^\circ$ in Fig. 1, and for the integrated loss function of TiO_2 in Fig. 3: in both cases RPA and TDLDA curves are almost indistinguishable. As a general rule, TDLDA correction are more pronounced when LFE have larger effects on the spectra (see e.g., the discussion of Fig. 15 in Ref. [14]). Accordingly, it works out that when the TDLDA approximation provides large improvements with respect to the independent-particle KS spectra, an essential contribution always comes from the density variation of the Hartree potential (LFE). In addition, we point out that TDLDA and RPA proved to be adequate to calculate loss functions in graphite, both when the system behaves like a solid (for in-plane $\boldsymbol{q}$) and when it shows features characteristic of isolated layers (for $\boldsymbol{q}$ along the c-axis).

On average, it is possible to conclude that the TDLDA approximation is often reliable for EELS at small momentum transfer in all kind of systems, and for absorption in finite systems, but not for absorption in extended systems.

4. Further developments

Presently, it would be extremely desirable to find better and generally applicable approximations for f_{xc}. Improvements of the description of quasiparticle and excitonic effects in absorption processes might come through the inclusion of dynamical (memory) effects and/or long-range nonlocal terms [6,27,28,34–37], completely absent in the TDLDA approximation. Starting from the consideration that good absorption spectra for solids can be calculated within many-body perturbation theory, thanks to Hedin's GW corrections for quasiparticle energies and the solution of the two-particle Bethe–Salpeter equation (BSE), Reining *et al.* [27] have shown that a *static* long-range contribution

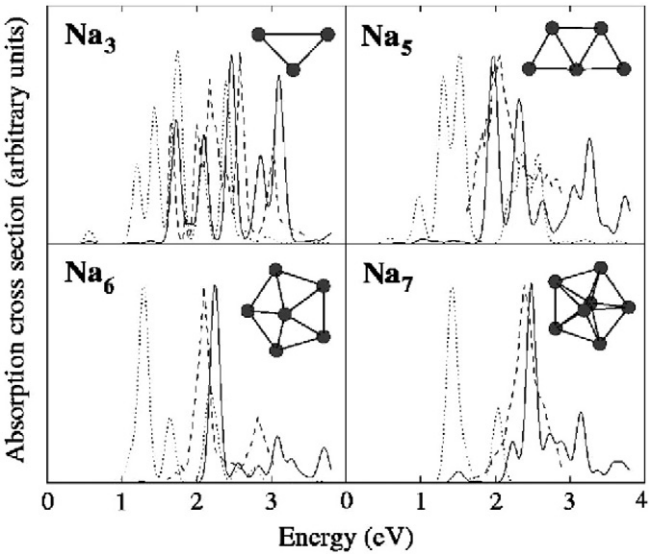

Fig. 5. Absorption spectra of Na_3, Na_5, Na_6, and Na_7 clusters from Ref. [31]. TDLDA calculations: (solid lines); IP-RPA spectra (dotted lines); experimental spectra: (dashed lines).

(LRC) of the form $f_{xc}(\boldsymbol{q}, \boldsymbol{G}, \boldsymbol{G}', \omega) = -\delta_{\boldsymbol{G},\boldsymbol{G}'}\alpha/|\boldsymbol{q}+\boldsymbol{G}|^2$ ($\boldsymbol{q}$ is a vector in the first Brillouin zone, $\boldsymbol{G}$ and $\boldsymbol{G}'$ are reciprocal lattice vectors, and α is a material dependent parameter) can simulate the strong continuum excitonic effect in the absorption spectrum of bulk semiconductors [28], provided that quasiparticle eigenvalues are used instead of LDA-KS eigenvalues in the construction of χ_0. This approximation for the xc-kernel, not necessarily very similar to the unknown exact kernel [37], yields a spectrum extremely close to the one obtained by solving the BSE.

Comparing Eq. (5) and Eq. (14), one can understand why in solids the long-range contribution is much more important for absorption than for electron energy loss spectra: in the former case, in Eq. (14) f_{xc} is added to a coulombian $\bar{v}$ which does not contain the long-range term, as $v(\boldsymbol{G}=0)$ is set to zero. Obviously in that case, a neglect of the divergence in f_{xc} makes an essential difference, whereas in the case of loss spectra, determined via Eq. (5), this argument does not hold. Similarly, we can understand that in a finite system a long-range term can never be relevant. In addition, this long-range approximation for the screened electron-hole interaction is expected (as it is proved in Ref. [28]) to work best for systems with weakly bound excitons (i.e. for semiconductors and not for wide gap materials). This does not mean that the excitonic effects themselves are weak, since the electron–hole interaction often drastically changes the spectral lineshape, as it happens for silicon. Indeed, let us go back to look at silicon absorption spectra in Fig. 4, for there are still some curves we need to comment on. The dashed curve is the result obtained by replacing KS eigenvalues with GW quasiparticle energies in the RPA form of ε. Again, we find the well-known discrepancies with experiment: now the calculated spectrum shows a blueshift and the intensity of the E_1 structure has not been corrected. Finally, the solid curve is the result of the LRC calculation, which is quite close to the BSE result (grey solid line). One adjustable parameter α is sufficient to correct both the peak positions and the intensities, which is far from trivial. Of course, the method is neither valid for all kinds of materials, nor for all

kinds of excitation spectra. Without forgetting the limitations of this approach, it is however possible to use it to predict optical properties of semiconductors, by just determining the one number α. In fact, it has been shown [28] that α is inversely proportional to the dielectric constant of the material. Comparable findings are presented in a recent work by Kim and Görling [36,38], where the absorption spectrum of bulk silicon is calculated in the framework of the "exact exchange" (EXX) formalism. Within EXX formalism, the authors obtain the KS band structure by means of an exchange potential V_x and then the dielectric function from an exchange kernel f_x, which presents the $1/r$ long-range behaviour. The neglection of correlation leads to a collapse of the spectrum: the inconvenience is solved by the introduction of an empirical cut-off for the Coulomb interaction, which simulates the missing screening. Further terms in the expansion of the xc-kernel, beyond the EXX f_x term, as well as contributions beyond $f_{xc} = -\alpha/q^2$ lead to a class of parameter-free kernels, which yield accurate optical spectra within a fully *ab initio* TDDFT [35].

In conclusion, I have examined some applications of TDDFT to the calculation of electron energy loss spectra, absorption spectra, and dielectric constants in finite and extended systems. I have discussed successive approximation levels in the formalism, associating the different contributions to their physical effects. This analysis leads to understand which terms are expected to produce a sizeable contribution to spectra, and thus have to be necessarily included in calculations. The case of the xc-kernel is particularly interesting, as a general expression for this term is unknown and the search for improved approximations is stimulating at present an extensive debate in the TDDFT community. Some recent breakthroughs concerning the description of absorption in solids are promising steps towards a generally applicable formalism for TDDFT, which will allow to explore those complex systems that are up to now out of reach for spectroscopic simulations.

Acknowledgments

I thank Apostolos Marinopoulos, Valerio Olevano, Lucia Reining, Francesco Sottile, and Nathalie Vast for their contributions. I am grateful to Lucia Reining for the careful reading of the manuscript. My work was supported by a Marie Curie Fellowship of the European Community, contract No. IHP-MPMF-CT-2002-01793, and by the RTN European Community contract NANOPHASE No. HPRN-CT-2000-00167.

References

1. Hohenberg, P. and Kohn, W., Phys. Rev. **136**, B864 (1964).
2. Kohn, W. and Sham, L. J., Phys. Rev. **140**, A1133 (1965).
3. See e.g., Rohlfing, M., Palummo, M., Onida, G. and Del Sole, R., Phys. Rev. Lett. **85**, 5440 (2000).
4. Runge, E. and Gross, E. K. U., Phys. Rev. Lett. **52**, 997 (1984).
5. Gross, E. K. U. and Kohn, W., Phys. Rev. Lett. **55**, 2850 (1985).
6. Gross, E. K. U., Dobson, F. J. and Petersilka, M., "Density Functional Theory," (Springer, 1996).
7. Casida, M. E., "Recent Advances in Density Functional Methods," (World Scientific, Singapore, 1995), (ed. by D. P. Chong).
8. Jensen, F., "Introduction to Computational Chemistry," (Wiley, Chichester, England, 1999), Chap. 4; Bonacić-Koutechky, V., Fantucci, P. and Koutechky, J., J. Chem. Phys. **93**, 3802 (1990); Szabo, A. and Ostlund, N. S., "Modern Quantum Chemistry," (MacMillan, New York, 1983).
9. Hedin, L., Phys. Rev. **139**, A796 (1965).
10. Hedin, L. and Lundqvist, B. I., J. Phys. C **4**, 2064 (1971).
11. Hanke, W. and Sham, L. J., Phys. Rev. Lett. **33**, 582 (1974); Hanke, W. and Sham, L. J. Phys. Rev. B **12**, 4501 (1975).
12. Hanke, W. and Sham, L. J., Phys. Rev. B **21**, 4656 (1980).
13. Onida, G., Reining, L., Godby, R. W., Del Sole, R. and Andreoni, W., Phys. Rev. Lett. **75**, 818 (1995); Albrecht, S., Reining, L., Del Sole, R., and Onida, G., Phys. Rev. Lett. **80**, 4510 (1998); Rohlfing, M. and Louie, S. G., Phys. Rev. Lett. **80**, 3320 (1998); Benedict L. X. and Shirley, E. L., Phys. Rev. B **59**, 5441 (1999).
14. Onida, G., Reining, L. and Rubio, A., Rev. Mod. Phys. **74**, 601 (2002), and references therein.
15. Adler, S. L., Phys. Rev. **126**, 413 (1962).
16. Wiser, N., Phys. Rev. **129**, 62 (1963).
17. Ehrenreich, H., in "The Optical Properties of Solids," (edited by J. Tauc), (Academic, New York, 1966), Proceedings of the International School of Physics "Enrico Fermi", course XXXIV, p. 106.
18. Baroni, S. and Resta, R., Phys. Rev. B **33**, 7017 (1986), and references therein.
19. Almbladh, C.-O. and Hedin, L., in "Handbook on Synchrotron Radiation," (North-Holland, Amsterdam, 1983), vol. 1, p. 607.
20. Petersilka, M., Gossmann, U. J. and Gross, E. K. U., Phys. Rev. Lett. **76**, 1212 (1996).
21. Hanke, W., Adv. Phys. **27**, 287 (1978).
22. Gross, E. K. U. and Kohn, W., Phys. Rev. Lett. **57**, 923 (1986).
23. Marinopoulos, A. *et al*., Phys. Rev. Lett. **89**, 076402 (2002).
24. Botti, S., Vast, N., Reining, L., Olevano, V. and Andreani, L. C., Phys. Rev. Lett. **89**, 216803 (2002).
25. Fiore, A., Berger, V., Rosencher, E., Bravetti, P. and Nagle, J., Nature **391**, 463 (1998).
26. Vast, N., Reining, L., Olevano, V., Schattschneider, P. and Jouffrey, B., Phys. Rev. Lett. **88**, 37601 (2002).
27. Reining, L., Olevano, V., Rubio, A. and Onida, G., Phys. Rev. Lett. **88**, 066404 (2002).
28. Botti, S. *et al*., (2003), submitted.
29. Louie, S. G., Chelikowsky, J. R. and Cohen, M. L., Phys. Rev. Lett. **34**, 155 (1975).
30. See e.g., Rubio, A. and Serra, L., Z. Phys. D: At., Mol. Clusters **26**, S11 (1993); Rubio, A., Alonso, J. A., Blase, X., Balbás, L. C. and Louie, S. G., Phys. Rev. Lett. **77**, 247 (1996); Rubio, A., Alonso, J. A., Blase, X. and Louie, S. G., Int. J. Mod. Phys. B **11**, 2727 (1997); Serra, L. and Rubio, A., Phys. Rev. Lett. **78**, 1428 (1997); Castro, A. *et al*., J. Chem. Phys. **118**, 1930 (2001); Yabana, K. and Bertsch, G. F., Phys. Rev. B **54**, 4484 (1996); Yabana, K. and Bertsch, G. F., Int. J. Quantum Chem. **75**, 55 (1999); Yabana, K. and Bertsch, G. F., Phys. Rev. A **60**, 1271 (1999).
31. Vasiliev, I., Oğüt, S. and Chelikowsky, J. R., Phys. Rev. B **65**, 115416 (2002).
32. Vasiliev, I., Oğüt, S. and Chelikowsky, J. R., Phys. Rev. Lett. **82**, 1919 (1999).
33. Olevano, V. and Reining, L., Phys. Rev. Lett. **86**, 5962 (2001).
34. Tokatly, I. V. and Pankratov, O., Phys. Rev. Lett. **86**, 2078 (2001).
35. Sottile, F., Olevano, V. and Reining, L., Phys. Rev. Lett. **91**, 056402 (2003).
36. Kim, Y. and Görling, A., Phys. Rev. Lett. **89**, 096402 (2002).
37. Del Sole, R., Adragna, G., Olevano, V. and Reining, L. (2003).
38. Kim, Y. and Görling, A., Phys. Rev. B **66**, 035114 (2002).

